Available online at www.sciencedirect.com
SCIENCE DIRECT®
International Journal of Thermal Sciences 45 (2006) 60–69
International Journal of Thermal Sciences
www.elsevier.com/locate/ijts

The effect of variable viscosity on mixed convection heat transfer along a vertical moving surface

Mohamed E. Ali

Department of Mechanical Engineering, King Saud University, PO Box 800, Riyadh 11421, Saudi Arabia

Received 11 December 2004; received in revised form 12 April 2005; accepted 12 April 2005

Available online 31 May 2005

Abstract

The effect of temperature dependent viscosity on laminar mixed convection boundary layer flow and heat transfer on a continuously moving vertical surface is studied. The fluid viscosity is assumed to vary as an inverse linear function of temperature. Local similarity solutions are obtained for the boundary layer equations subject to isothermally moving vertical surface with uniform speed. The effect of various governing parameters, such as Prandtl number Pr, the mixed convection parameter $\lambda = S\,Gr_x/Re_x^2$, and the viscosity/temperature parameter θ_r which determine the velocity and temperature distributions, the local heat transfer coefficient, and the local shear stress coefficient at the surface are studied. Significant changes are obtained in dimensionless local heat transfer and shear stress coefficient at the surface when the magnitude of θ_r has small values for each λ. Critical values of λ are obtained for predominate natural convection and buoyancy shear stress for assisting and opposing flow for various θ_r.

Keywords: Mixed convection; Moving surface; Local similarity; Boundary layers; Skin friction coefficient; Variable viscosity

1. Introduction

Continuously moving surface through an otherwise quiescent medium has many applications in manufacturing processes. Such processes are hot rolling, wire drawing, spinning of filaments, metal extrusion, crystal growing, continuous casting, glass fiber production, and paper production [1–3].

Since the pioneer study of Sakiadis [4] who developed a numerical solution for the boundary layer flow field of a stretched surface, many authors have attacked this problem to study the hydrodynamic and thermal boundary layers due to a moving surface [5–14].

Suction or injection of a stretched surface was introduced by Erickson et al. [15] and Fox et al. [16] for uniform surface velocity and temperature and by Gupta and Gupta [17] for linearly moving surface. Chen and Char [18] have studied the suction and injection on a linearly moving plate subject to uniform wall temperature and heat flux and the more general case using a power law velocity and temperature distribution at the surface was studied by Ali [19]. Magyari et al. [20] have reported analytical and computational solutions when the surface moves with rapidly decreasing velocities using the self-similar method.

In all papers cited earlier the effect of buoyancy force was relaxed and the following papers have taken it into consideration. Such papers are those of Lin et al. [21], Ali and Al-Yousef [22–24], Chen [25,26], and by Ali [27].

To date, researchers have only considered the effect of constant viscosity on boundary layer developed by a continuously moving surface. However, it is known that the fluid viscosity changes with temperature [28] for example the absolute viscosity of water decreases by 240% when the temperature increases from 10 °C to 50 °C. Furthermore, Pop et al. [29], and Elbashbeshy and Bazid [30] have studied the effect of variable viscosity using the similarity solution with no buoyancy force.

Therefore, in order to get more accurate information about the flow and temperature profiles the present paper in-

E-mail address: mali@ksu.edu.sa (M.E. Ali).

1290-0729/$ – see front matter
doi:10.1016/j.ijthermalsci.2005.04.006

Nomenclature

a	constant
f	dimensionless stream function
Gr_x	Grashof number $(g\beta(T_w - T_\infty)x^3/\nu^2$
k	thermal conductivity
Nu_x	Nusselt number (hx/k)
Pr	Prandtl number (ν/α)
Re_x	Reynolds number $(U_w x/\nu_\infty)$
S	dummy parameter
T	temperature
T_r	viscosity reference temperature
u	velocity component in x-direction
v	velocity component in y-direction
x	coordinate in direction of surface motion
y	coordinate in direction normal to surface motion

Greek symbols

α	thermal diffusivity
β	thermal expansion coefficient
γ	constant
η	similarity variable
θ	dimensionless temperature
θ_r	dimensionless reference temperature
λ	buoyancy parameter $(S\,Gr_x/Re_x^2)$
μ	absolute viscosity
ν	kinematic viscosity
ρ	density

Subscripts

w	condition at the surface
∞	condition at ambient medium

vestigates the effect of viscosity variation with temperature on mixed convection boundary layer adjacent to a continuously moving vertical surface. However, the analyses are focused on the case of uniformly moving isothermal surface for different Prandtl numbers corresponding to water and air using the local similarity approach.

The mathematical formulation of the problem is presented in Section 2, followed by numerical solution procedure in Section 3. Results and discussion are presented in Section 4, and finally conclusions are given in Section 5.

2. Mathematical analysis

Consider the laminar steady two-dimensional motions of mixed convection boundary layer flow due to a vertically moving isothermal surface. Using Boussinesq approximation for incompressible viscous fluid environment in addition to that, the fluid viscosity is assumed to vary as an inverse linear function of temperature (Ling and Dybbs [31], and Lai and Kulacki [32]):

$$\frac{1}{\mu} = \frac{1}{\mu_\infty}\big[1 + \gamma(T - T_\infty)\big], \quad \text{or} \quad \frac{1}{\mu} = a(T - T_r) \tag{1}$$

where

$$a = \frac{\gamma}{\mu_\infty} \quad \text{and} \quad T_r = T_\infty - \frac{1}{\gamma} \tag{2}$$

are constants, and their values depend on the reference state of the fluid. In general, it can be seen that for liquids and gases a is > 0 and < 0, respectively [31]. It should be mentioned that the above model has used by Hossain et al. [33] and Hossain and Munir [34] in studying natural convection from a vertical wavy cone and the mixed convection from a vertical flat plate respectively.

The equations governing this convective variable viscosity fluid flow are

$$\frac{\partial u}{\partial x} + \frac{\partial v}{\partial y} = 0 \tag{3}$$

$$u\frac{\partial u}{\partial x} + v\frac{\partial u}{\partial y} = Sg\beta(T - T_\infty) + \frac{1}{\rho_\infty}\frac{\partial}{\partial y}\left(\mu\frac{\partial u}{\partial y}\right) \tag{4}$$

$$u\frac{\partial T}{\partial x} + v\frac{\partial T}{\partial y} = \alpha\frac{\partial^2 T}{\partial y^2} \tag{5}$$

subject to the following boundary conditions:

$$\begin{aligned} &u = U_w, \quad v = 0 \quad @\ y = 0\\ &T = T_w \quad @\ y = 0\\ &u \to 0, \quad T \to T_\infty \quad @\ y \to \infty \end{aligned} \tag{6}$$

The x coordinate is measured along the moving surface from the point where the surface originates, and the y coordinate is measured normal to it (Fig. 1). Where, u and v are the velocity components in x- and y-directions respectively and S is a dummy parameter stands for 0, $+1$, or -1. Using the stream function ψ and the following transformation:

$$\psi = \sqrt{2}\nu_\infty Re_x^{1/2} f(\eta), \qquad \eta = \frac{y}{x\sqrt{2}} Re_x^{1/2} \tag{7}$$

$$\theta(\eta) = \frac{(T - T_\infty)}{(T_w - T_\infty)} \tag{8}$$

where

$$u = \frac{\nu_\infty}{x} Re_x f'(\eta), \qquad Re_x = \frac{U_w x}{\nu_\infty}$$

$$v = \frac{\nu_\infty Re_x^{1/2}}{x\sqrt{2}}(f'\eta - f) \tag{9}$$

where f' and θ are the dimensionless velocity and temperature respectively, and η is the similarity variable. Substitution in the governing equations (4), (5) gives rise to the following local similarity two-point boundary-value problem

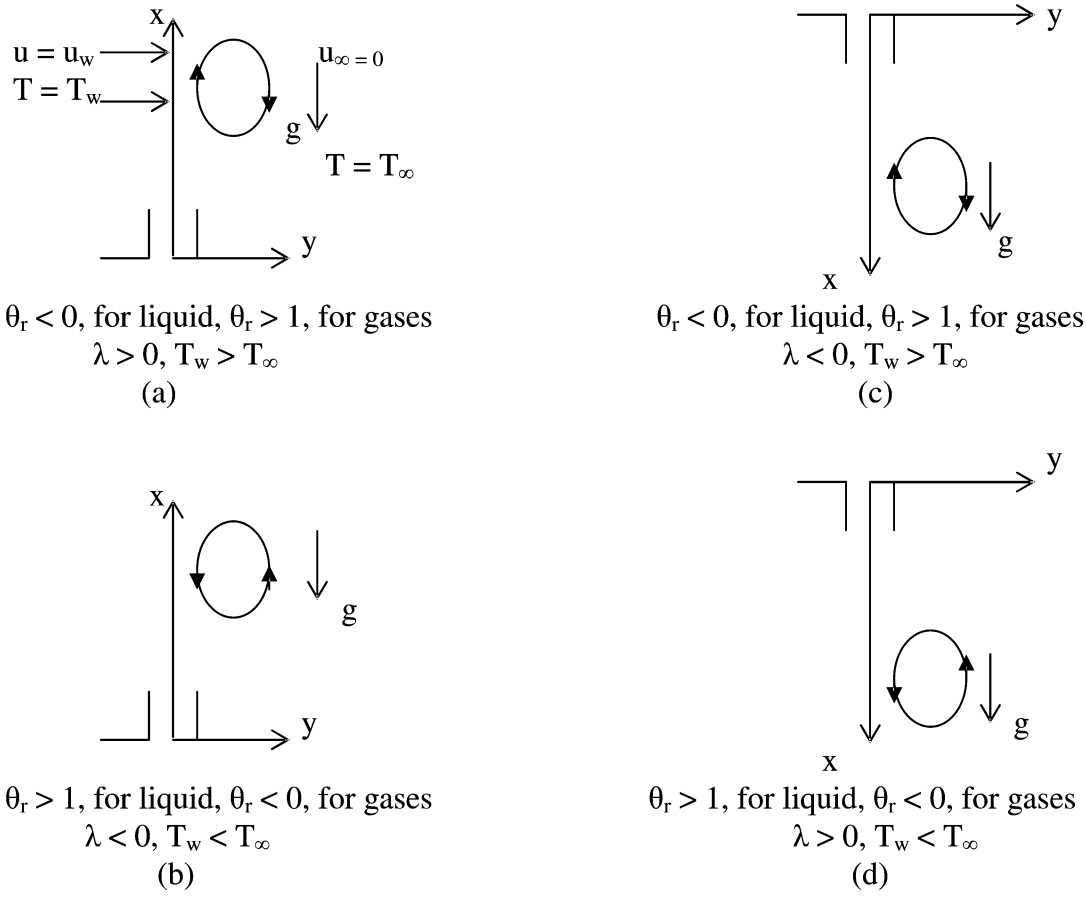

Fig. 1. Schematic of the physical problem of moving surface from a slot: (a) the surface is moving upwards in the x direction and the buoyancy force assisting the flow, (b) the same as but the buoyancy force opposing the flow, (c) the surface is moving downwards and the buoyancy force opposing the flow, and (d) the same as (c) but the buoyancy force assisting the flow.

$$f''' - \frac{(\theta-\theta_r)}{\theta_r} f f'' - \frac{1}{(\theta-\theta_r)}\theta' f'' - \frac{2\lambda(\theta-\theta_r)}{\theta_r}\theta = 0 \tag{10}$$

$$\theta'' + Pr\, f\theta' = 0 \tag{11}$$

The transformed Boundary conditions are

$$f'(0) = 1, \qquad f(0) = 0, \qquad \theta(0) = 1$$
$$f'(\infty) \to 0, \qquad \theta(\infty) \to 0 \tag{12}$$

where, θ_r is a constant viscosity/temperature parameter defined by

$$\theta_r = \frac{T_r - T_\infty}{T_w - T_\infty} = -\frac{1}{\gamma(T_w - T_\infty)} \tag{13}$$

The last term in Eq. (10) is due to the buoyancy force and $\lambda = SGr_x/Re_x^2$ which, serves as the buoyancy parameter and $Gr_x = g\beta(T_w - T_\infty)x^3/\nu^2$, when $S = 0$ implies $\lambda = 0$ that means the buoyancy forces are neglected and the governing equations (10), (11) reduce to those of forced convection limit obtained by Pop et al. [29] (when the same definition of similarity variable is used) and by Elbashbeshy and Bazid [30]. It should be mentioned that, when $\gamma = 0$ then $\theta_r \to \infty$ and Eq. (10) reduces to those of constant viscosity of Sakiadis [4]. Furthermore, Eqs. (10), (11) reduce to Ali [10,19] for no buoyancy force and for Ali and Al-Yousef [22–24] when the buoyancy force included. It should be noted that λ is a function of x and Eq. (10) contains x, therefore the local similarity approach (Kays and Crawford [35]) is applied to solve the governing Eqs. (10), (11). Furthermore, local similarity approach implied that the dimensionless quantities (Gr_x, Re_x, Nu_x) are determined locally at any x-station and the upstream history of the flow is ignored, except as it influences the similarity variable.

Moreover, It can be shown [30] that for $(T_w - T_\infty) > 0$, θ_r must physically be > 1 for gases and < 0 for liquids. However, the opposite is true if $(T_w - T_\infty) < 0$, where θ_r must physically be > 1 for liquids and < 0 for gases. Furthermore, Fig. 1 shows all physical considerations of θ_r $(T_w - T_\infty)$, and λ when the vertical surface is moving either upwards or downwards. It worth mentioning that, when $S = +1$ and $T_w > T_\infty$ $(\lambda > 0)$ means that the x-axis points upwards in the direction of stretching surface such that the stretching induced flow and the thermal buoyant flow assist each other (assisting flow, Fig. 1(a)). On the other hand, when $S = -1$ and $T_w > T_\infty$ $(\lambda < 0)$ means that the x-axis points vertically downwards in the direction of stretching surface but in this case the stretching induced flow and the thermal buoyant flow oppose each other (opposing flow, Fig. 1(c)). Furthermore, the opposite is absolutely true if $T_w < T_\infty$, where the

first case is $S = +1$ ($\lambda < 0$) and the x-axis points upwards (opposing flow, Fig. 1(b)) and the second case is $S = -1$ ($\lambda > 0$) and the x-axis points downwards (assisting flow, Fig. 1(d)).

The local shear stress at the surface can be expressed in a dimensionless form of the skin friction coefficient as

$$C_f \sqrt{Re}_x = \frac{\sqrt{2}\theta_r}{(\theta_r - 1)} f''(0, \theta_r) \tag{14}$$

and the local heat transfer coefficient in terms of Nusselt number is expressed as

$$\frac{Nu_x}{\sqrt{Re}_x} = -\frac{1}{\sqrt{2}} \theta'(0, \theta_r) \tag{15}$$

3. Numerical solution procedure

The coupled nonlinear ordinary differential equations (10) and (11) are solved numerically by using the fourth order Runge–Kutta method. Local similarity solutions of the differential Eqs. (10), (11) subject to the boundary conditions (12) were obtained for increasing values of λ at each constant θ_r. At each new θ_r we start from a known solution of the equations with $\lambda = 0$ (Pop et al. [29]) where $f''(0)$ and $\theta'(0)$ are known. For a given value of λ the values of $f''(0)$ and $\theta'(0)$ were estimated and the differential equations (10) and (11) were integrated using Runge–Kutta method until the boundary conditions at infinity $f'(\infty)$ and $\theta(\infty)$ decay exponentially to zero ($\leqslant 10^{-4}$ where the solution to be accepted and solutions with $f'(\infty)$ and $\theta(\infty) > 10^{-4}$ will not be considered). If the boundary conditions at infinity are not satisfied then the numerical routine uses a half interval method to calculate corrections to the estimated values of $f''(0)$ and $\theta'(0)$. This process is repeated iteratively until exponentially decaying solution in f' and θ is obtained. The value of η_∞ was chosen as large as possible between 3.5 and 25 depending upon the Prandtl number and the viscosity/temperature parameter θ_r, without causing numerical oscillations in the values of f' and θ. The local solutions were obtained for different values of $-10 \leqslant \theta_r \leqslant 10$. It should be noted that numerical solutions have become more difficult to obtain as λ increases and $\lambda_{\max}$ is the maximum value of λ which can be obtained (where the solution could be obtained and satisfying the accuracies mentioned earlier) at the corresponding θ_r and Pr. Comparisons are made quantitatively with Pop et al. [29] for $\lambda = 0$ in Table 1 in terms of $f''(0)$ and $\theta'(0)$ for $Pr = 0.7$ (using the same expression of η defined by [29] with rescaled current equations (10) and (11) to be consistent) which show good agreement with the present results. It should be noted that, the differences in $\theta'(0)$ at some θ_r appear in Table 1 is due to using large η than those mentioned in [29] such that $f'(\eta)$ and $\theta(\eta)$ profiles go asymptotically to zero.

Table 1
Comparison of $f''(0)$ and $\theta'(0)$ to previously published data at $Pr = 0.7$ and $\lambda = 0$ for different values of θ_r using the same expression of $\eta = \frac{y}{x} Re_x^{1/2}$ defined by [29] with rescaled Eqs. (10) and (11) to be consistent

θ_r		Pop et al. [29]	Present results
−8.0	$f''(0)$	−0.4773578	−0.4763230
	$\theta'(0)$	−0.3493189	−0.3432339
−0.1	$f''(0)$	−1.5061732	−1.4965150
	$\theta'(0)$	−0.2191391	−0.1652394
−0.01	$f''(0)$	−4.4856641	−4.4683560
	$\theta'(0)$	−0.1544918	−0.0561845
−0.001	$f''(0)$	−14.0654213	−14.042370
	$\theta'(0)$	−0.1340890	−0.0179588
8.0	$f''(0)$	−0.4089153	−0.4083475
	$\theta'(0)$	−0.3605226	−0.3555822

4. Results and discussion

Eqs. (10) and (11) were solved numerically, as described in Section 3, for $-10 \leqslant \theta_r \leqslant 10$, $Pr = 0.72, 3, 7$, and for various values of λ where the surface is moving upwards or downwards corresponding to the matrix given in Fig. 1. Samples of the resulting velocity and temperature profiles for $Pr = 0.72$ (air) and for different values of θ_r and λ are presented in Figs. 2 and 3. Fig. 2(a) shows the velocity profiles for $\theta_r < 0$ where surface moves downwards with $T_w < T_\infty$. As the magnitude of θ_r decreases, where the effect of viscosity is significant, for large values of λ ($\lambda = 5$) results in a relative rise in the velocity profiles (velocity overshoot) near the wall. However, the opposite is true for small values of λ ($\lambda = 0.01$ or 0). Fig. 2(b) shows the velocity variation for positive values of θ_r and for different values of λ where the hot surface is moving upwards. In this figure as in Fig. 2(a) as $|\theta_r|$ increases the profiles approach to that of constant viscosity case and as λ increases the velocity overshoot near the wall. Furthermore, the velocity boundary layer is thicker for positive than for negative θ_r. Fig. 3(a), (b) shows the temperature profiles for the same parameters and conditions mentioned in Fig. 2(a), (b). It is clear that these profiles are significantly influenced by the values of θ_r and λ. The effect of variable viscosity is to thicken the thermal boundary layer for $\theta_r < 0$ as θ_r approaches zero (Fig. 3(a)) while it is suppressed for $\theta_r > 1$ as θ_r approaches unity (Fig. 3(b)) for small values of λ. However, as λ increases these profiles are almost squeezed together making the gradient at the surface insignificant with changing θ_r in other words, the effect of viscosity change is overcome by the effect of buoyancy. As λ increases more, the relation between the thermal boundary layer and θ_r explained earlier is switched as seen in Fig. 3(b) for $\lambda = 20$. It worth mentioning that, similar results are obtained for other Prandtl numbers.

Local distributions of $Nu_x Re_x^{-1/2}$ at the surface for positive and negative θ_r (where the surface is moving upwards and downwards respectively) are presented in Fig. 4 for $Pr = 0.72$ and for different values of λ. It should be men-

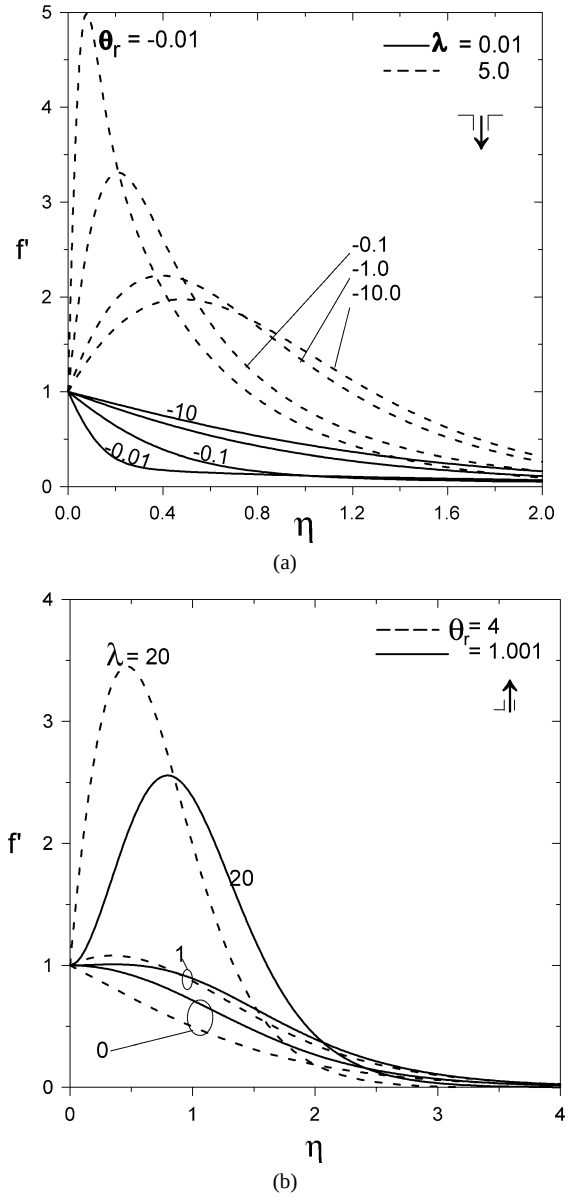

Fig. 2. Samples of velocity profiles for $Pr = 0.72$ and for different values of θ_r showing the effect of variable viscosity for buoyancy assisting flow: (a) the surface is moving downwards as in Fig. 1(d), (b) the surface is moving upwards as in Fig. 1(a).

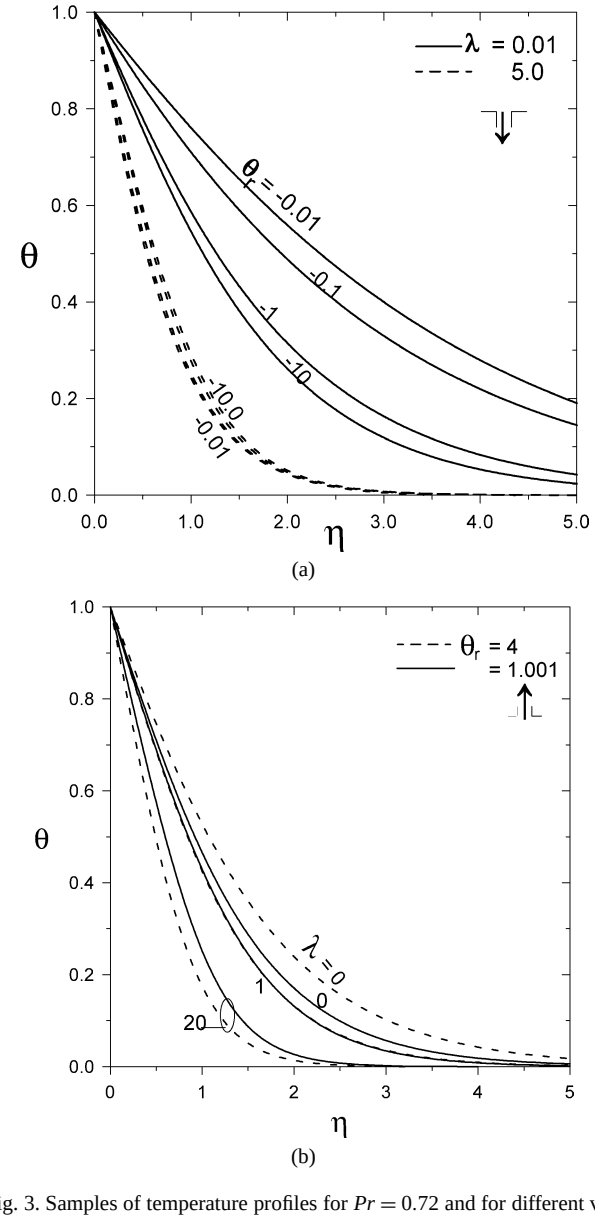

Fig. 3. Samples of temperature profiles for $Pr = 0.72$ and for different values of θ_r showing the effect of variable viscosity for buoyancy assisting flow: (a) the surface is moving downwards as in Fig. 1(d), (b) the surface is moving upwards as in Fig. 1(a).

tioned that, for gases where $\theta_r > 1$ or $\theta_r < 0$ corresponding to either heat transfers from the surface to the medium or the opposite respectively. However, for liquids the opposite is true. For this Prandtl number there are no solutions obtained satisfying the governing equations and the boundary conditions for $1.001 > \theta_r > -0.005$, and this area is marked in Fig. 4 between the vertical dashed lines. It can be seen from this figure that, there is a competition between the buoyancy force and the viscosity effect, i.e. for $\lambda = 0$ the effect of variable viscosity model is significant in reducing or increasing $Nu_x Re_x^{-0.5}$ for negative or positive θ_r respectively. As λ increases up to about 0.5 ($\theta_r < 0$) or 1 ($\theta_r > 1$) the two effects are almost balanced and $Nu_x Re_x^{-0.5}$ is unaffected by the variation of the fluid viscosity. It is observed that as λ increases more for $\theta_r < 0$ the local heat transfer is increased considerably as $\theta_r \to 0$ however, it is reduced as $\theta_r \to 1$ for $\theta_r > 1$. Furthermore, as $\theta_r \to \pm\infty$, $Nu_x Re_x^{-0.5}$ profiles asymptotically approach that of constant viscosity case ($\mu = \text{const.}$ lines), which means that the variation of fluid viscosity is negligible.

Fig. 5 shows the Nusselt number distributions for $Pr = 0.72$ for positive and negative θ_r for the entire mixed convection regime. As seen from the figure the buoyancy parameter effect is significant as $\theta_r \to 0$ for $\theta_r < 0$ where the Nusselt number profile is almost linear at $\theta_r = -0.01$. It worth mentioning that, for $\lambda > 0.5$, the Nusselt number profiles switch the order where the buoyancy effect dominates. The region

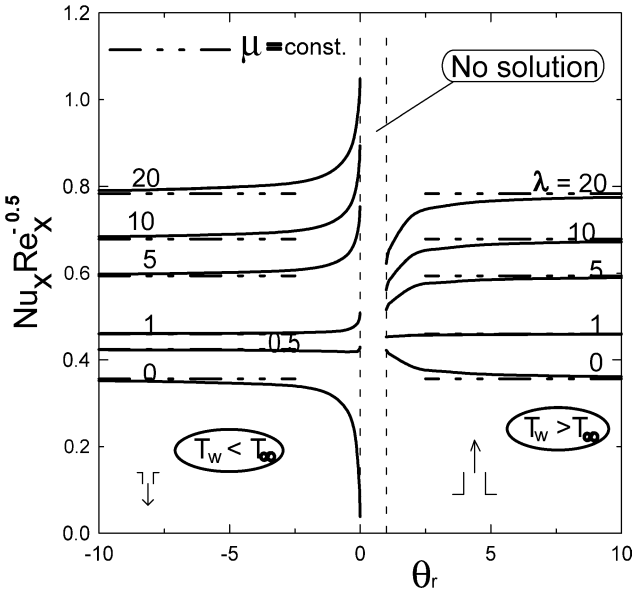

Fig. 4. Local Nusselt number distributions for $Pr = 0.72$ and for different values of λ for buoyancy assisting flow showing the region of no solution.

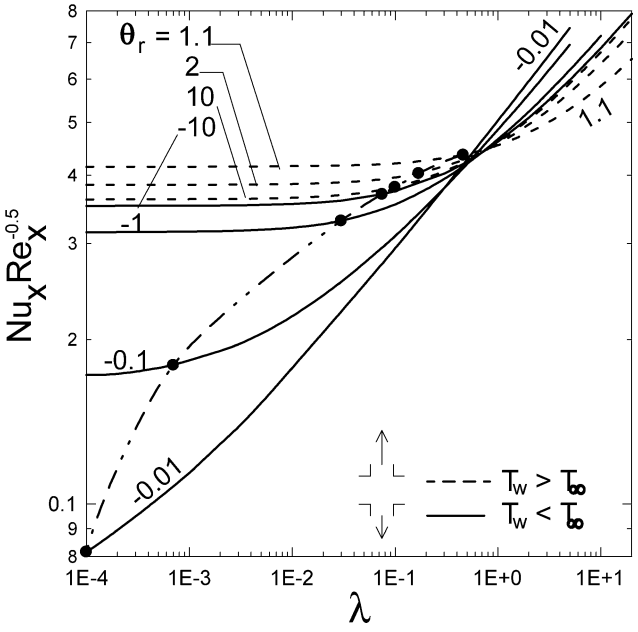

Fig. 5. Local Nusselt number distributions for the entire mixed convection for $0 > \theta_r > 1$ and $Pr = 0.72$. Dotted–dashed line presents the locus separating the natural convection dominant region on the right and the forced convection region on the left for buoyancy assisting flow.

of predominate natural convection is determined by taking 5% increase in Nusselt number of that at forced convection limit ($\lambda = 0$). The corresponding values of λ (which we call it critical values $\lambda_{(crt)c}$ are tabulated in Table 2 for each θ_r and for different Prandtl numbers. These critical values are presented as dotted–dashed line connecting the • symbols for $1 < \theta_r < 0$ and it should be reminded that there are no solutions for $1 > \theta_r > 0$. Therefore, the region on the right of this line presents the natural convection dominates whereas

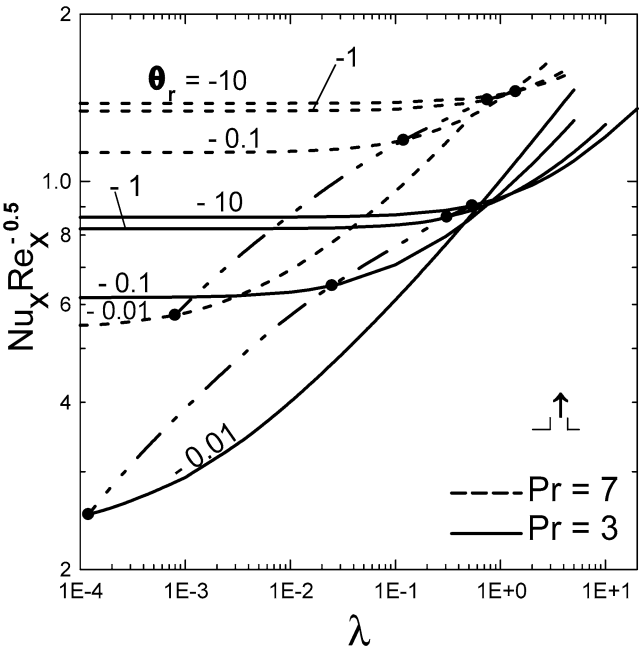

Fig. 6. Local Nusselt number distribution for the entire mixed convection for $\theta_r < 0$ for $Pr = 3$ and 7. Dotted–dashed lines present the locus separating the natural convection dominant region on the right and the forced convection region on the left for buoyancy assisting flow.

Table 2
Critical values of buoyancy assisting flow $\lambda_{(crt.)c}$ for predominate natural convection and the corresponding $Nu_x Re_x^{-1/2}$ for $Pr = 0.72$, 3, and 7 for various values of θ_r

θ_r	$Pr = 0.72$		$Pr = 3.0$		$Pr = 7.0$	
	$\lambda_{(crt.)c}$	$\frac{Nu_x}{Re_x}$	$\lambda_{(crt.)c}$	$\frac{Nu_x}{\sqrt{Re_x}}$	$\lambda_{(crt.)c}$	$\frac{Nu_x}{\sqrt{Re_x}}$
10.0	0.10	0.38005	0.65	0.91496	1.65	1.46225
7.0	0.10	0.38153	0.68	0.91754	1.72	1.46490
4.0	0.11	0.38684	0.75	0.92335	1.91	1.47130
2.0	0.17	0.40311	1.04	0.93984	2.6	1.48800
1.1	0.46	0.43545	2.37	0.96999	5.8	1.51704
−0.01	1e−4	0.07782	12e−5	0.25104	8e−4	0.57482
−0.1	7e−4	0.17893	0.025	0.64895	0.12	1.18596
−0.5	0.014	0.29738	0.19	0.82576	0.54	1.36697
−1.0	0.03	0.33003	0.31	0.86345	0.75	1.40225
−4.0	0.061	0.36118	0.48	0.89603	1.25	1.44283
−7.0	0.07	0.36656	0.52	0.90138	1.35	1.44853
−10	0.075	0.36896	0.54	0.90373	1.40	1.45108

the region on the left presents the domain of forced convection.

Local Nusselt number distributions for different values of θ_r and for $Pr = 3, 7$ are shown in Fig. 6 where the surface is moving upwards. In this figure, it is cleat that $Nu_x Re_x^{-1/2}$ is independent of λ in the forced convection domain on the left of the dotted–dashed lines and it is a function of θ_r only. Furthermore, increasing Prandtl number enhances the heat transfer coefficient for all values of θ_r. The critical values of predominate natural convection for both Prandtl numbers are tabulated in Table 2 as described earlier. It worth mentioning that, the numerical solution for $\theta_r = -0.01$ and $Pr = 7$ can-

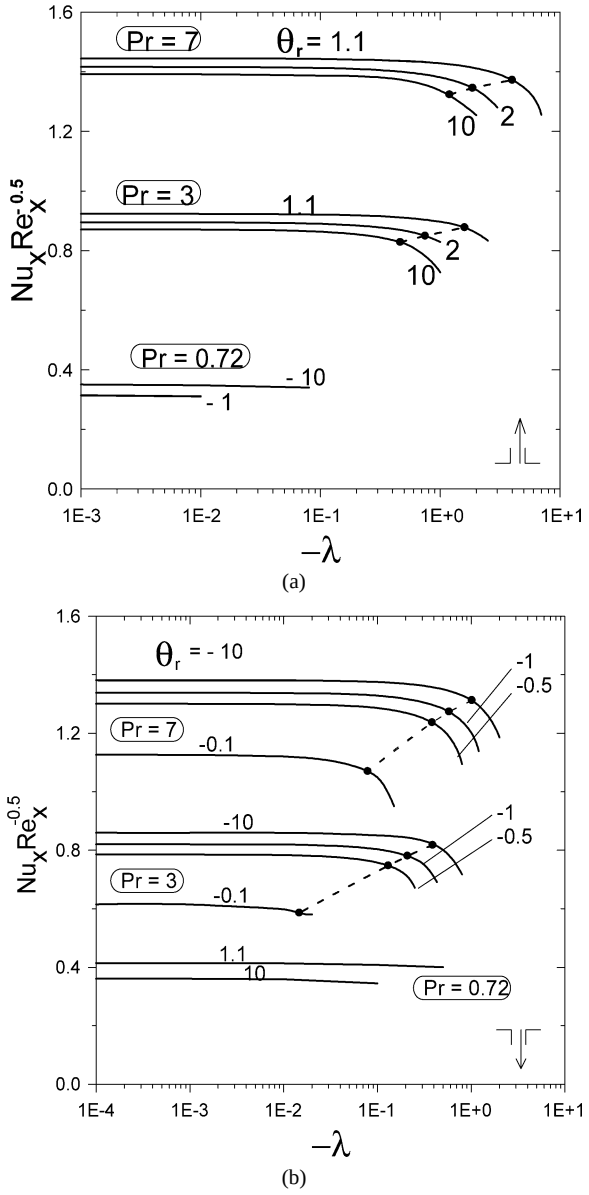

Fig. 7. Local Nusselt number distribution for the entire mixed convection for all $Pr = 0.72$, 3 and 7. Dashed lines present the locus separating the natural convection dominant region on the right and the forced convection region on the left for buoyancy opposing flow: (a) the surface is moving upwards as in Fig. 1(b), (b) the surface is moving downwards as in Fig. 1(c).

not be obtained for higher values of λ since the solution has a lower accuracies and has been rejected.

In Figs. 4–6, the buoyancy effect is to assist the flow, this means that $Nu_x Re_x^{-0.5}$ increases as λ increases according to the matrix Fig. 1(a), (d). Comparisons of $Nu_x Re_x^{-0.5}$ distributions at the surface for different Prandtl numbers where the buoyancy force opposing the flow, as sketched in Figs. 1(b), (c), are shown in Fig. 7(a), (b). In Fig. 7(a) the surface is moving upwards with $T_w < T_\infty$ and in Fig. 7(b) the hot surface is moving downwards. Dashed lines connecting the locus of predominate natural convection for $Pr = 3$ and 7 whereas these critical values are tabulated in Table 3. In Fig. 7(a), (b) $Nu_x Re_x^{-0.5}$ is reduced as $\theta_r \to 0$ for $\theta_r < 0$

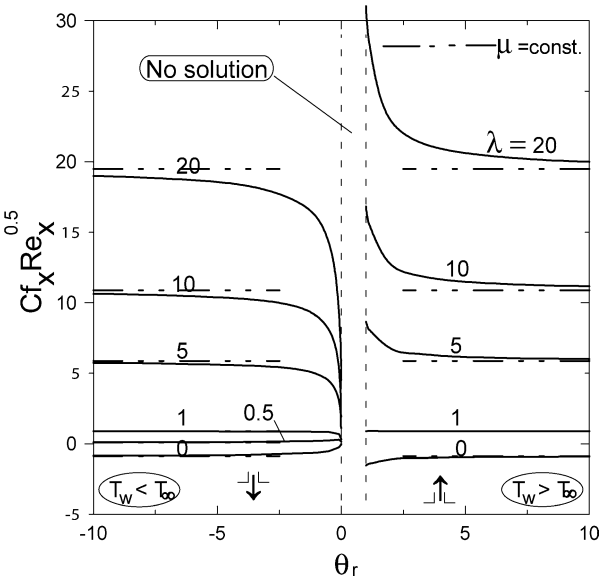

Fig. 8. Local skin friction coefficient profiles for $Pr = 0.72$ and for different values of λ for buoyancy assisting flow showing the region of no solution.

Table 3
Critical values of buoyancy opposing flow $\lambda_{(crt.)c}$ for predominate natural convection and the corresponding $Nu_x Re_x^{-1/2}$ for $Pr = 3$, and 7 for various values of θ_r

θ_r	$Pr = 3.0$			$Pr = 7.0$		
	$f''(0)$	$\lambda_{(crt.)c}$	$\frac{Nu_x}{\sqrt{Re_x}}$	$f''(0)$	$\lambda_{(crt.)c}$	$\frac{Nu_x}{\sqrt{Re_x}}$
10.0	−0.9484367	−0.466	0.82769	−1.209322	−1.2	1.32345
7.0	−0.9214851	−0.48	0.83058	−1.183714	−1.25	1.32564
4.0	−0.8655953	−0.541	0.83592	−1.113357	−1.39	1.33146
2.0	−0.7056180	−0.75	0.84931	−0.9140071	−1.87	1.34565
1.1	−0.2153614	−1.6	0.87825	−0.2979634	−4.0	1.37223
−0.1	−2.373538	−0.0147	0.58593	−2.882698	−0.079	1.06949
−0.5	−1.552044	−0.131	0.74710	−1.953567	−0.385	1.23682
−1.0	−1.335320	−0.21	0.78046	−1.681409	−0.58	1.27328
−4.0	−1.103024	−0.345	0.81065	−1.390445	−0.9	1.30630
−7.0	−1.059178	−0.375	0.81574	−1.344756	−0.983	1.31078
−10	−1.042438	−0.39	0.81760	−1.325513	−1.02	1.31260

but increased as $\theta_r \to 1$ for $\theta_r > 1$. It should be mentioned that for $Pr = 0.72$ forced convection dominates since there are no solutions obtained by the present method for natural convection dominates.

Now turning our attentions to the effect of viscosity temperature dependent on skin friction coefficient at the surface presented by $C_f Re^{0.5}$ for $Pr = 0.72$ as shown in Fig. 8 for the same parameters used in Fig. 4. Therefore, the competition between the buoyancy force and the viscosity temperature dependent for $\lambda = 0$ tends to increase or decrease $C_f Re^{0.5}$ for negative or positive θ_r respectively. As λ increases up to about 0.5 ($\theta_r < 0$) or 1 ($\theta_r > 1$) the two effects are almost balanced and $C_f Re^{0.5}$ is unaffected by the variation of the fluid viscosity. In addition, as λ increases more for $\theta_r < 0$, the local skin friction coefficient is reduced considerably as $\theta_r \to 0$ due to a decrease in the fluid viscosity where $\mu \to 0$. On the other hand, it is increased as

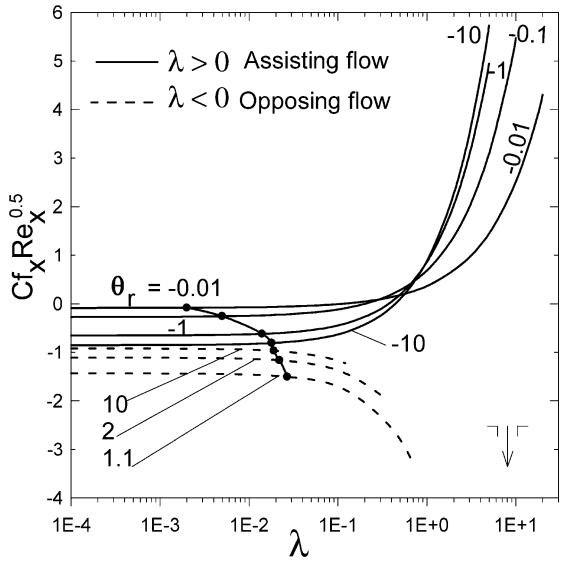

Fig. 9. The effect of buoyancy assisting and opposing flow on the dimensionless skin friction coefficient distributions at the surface for $Pr = 0.72$ for different values of λ_r. Line connecting • symbols indicates the predominate buoyancy assisting and opposing flow.

Table 4
Critical values of $\lambda_{(\mathrm{crt.})s}$ for predominate buoyancy assisting shear stress at the surface and the corresponding $C_f Re^{0.5}$ for $Pr = 0.72$, 3, and 7.0 for various values of θ_r

θ_r	$Pr = 0.72$		$Pr = 3.0$		$Pr = 7.0$	
	$\lambda_{(\mathrm{crt.})s}$	$C_f Re^{0.5}$	$\lambda_{(\mathrm{crt.})s}$	$C_f Re^{0.5}$	$\lambda_{(\mathrm{crt.})s}$	$C_f Re^{0.5}$
10.0	0.018	−0.88053	0.039	−0.86765	0.058	−0.86153
7.0	0.0195	−0.89342	0.40	−0.87771	0.059	−0.86911
4.0	0.021	−0.93419	0.41	−0.90603	0.06	−0.88983
2.0	0.022	−1.05793	0.0428	−0.98099	0.062	−0.94272
1.1	0.0275	−1.36130	0.048	−1.13574	0.073	−1.03924
−0.01	0.002	−0.08358	0.003	−0.08496	0.006	−0.08526
−0.1	0.005	−0.25914	0.015	−0.27270	0.025	−0.30040
−0.5	0.0115	−0.50789	0.028	−0.55448	0.045	−0.59879
−1.0	0.014	−0.62222	0.035	−0.66183	0.05	−0.69879
−4.0	0.017	−0.77094	0.037	−0.78877	0.055	−0.80173
−7.0	0.018	−0.79922	0.038	−0.81071	0.056	−0.81896
−10.0	0.018	−0.81224	0.038	−0.82034	0.057	−0.82560

$\theta_r \to 1$ for $\theta_r > 1$ due to an increase in the fluid viscosity where $\mu \to \infty$. A further increase in the fluid viscosity ($\theta_r < 1$) will result in an adverse pressure gradient since f' will approach a constant value of 1 as approximately seen in Fig. 2(b) for $\theta_r = 1.001$. Therefore, separation of flow will occur and the boundary layer assumptions fails and the local similarity solutions no longer exist which ensures that there is no solution for $0 \leqslant \theta_r \leqslant 1$ as seen in Figs. 4 and 8 (see [19,32,35,36] for similar cases). Furthermore, as $\theta_r \to \pm\infty$, $C_f Re^{0.5}$ profiles asymptotically approach that of constant viscosity case ($\mu = $ const. lines), which means that the variation of fluid viscosity is negligible.

Fig. 9 presents the $C_f Re^{0.5}$ profiles for $Pr = 0.72$ where the buoyancy assisting or opposing the flow for negative and positive θ_r, respectively. A 5% increase or decrease in

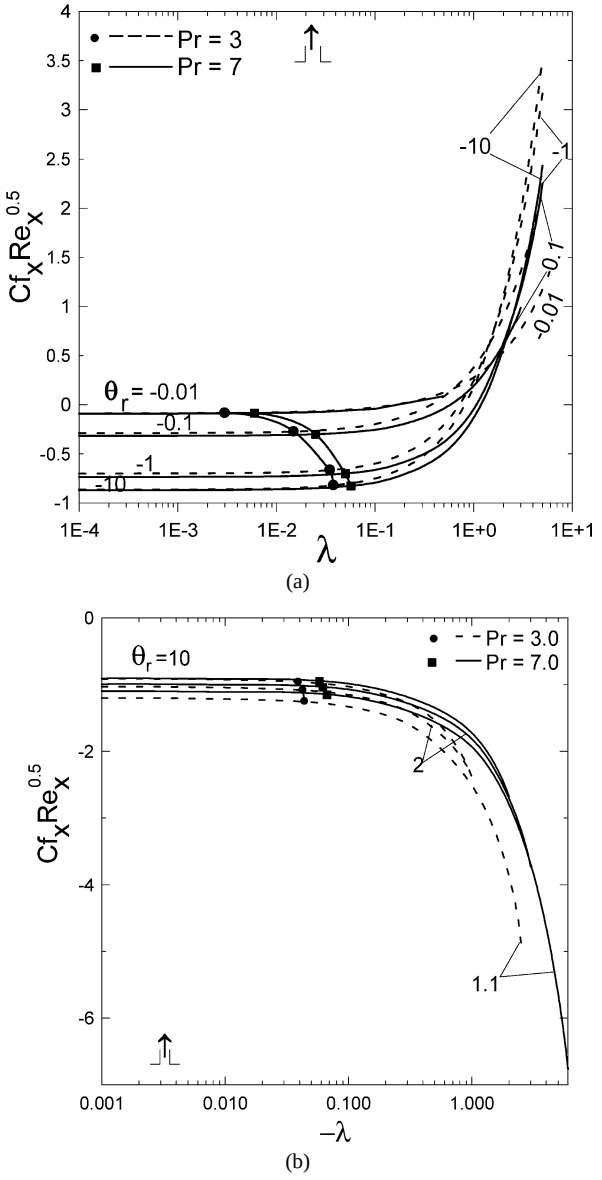

Fig. 10. Dimensionless skin friction coefficient distributions at the surface for $Pr = 3$ and 7: (a) buoyancy assisting flow, (b) buoyancy opposing flow.

$C_f Re^{0.5}$ at $\lambda = 0$ (Forced convection only) has been applied to see the effect of buoyancy. The solid line connecting • symbols present those values of 5% increase or decrease. The predominate buoyancy effect region on the shear stress is on the right of this line. The numerical values of λ which we call it $\lambda_{(\mathrm{crt.})s}$ corresponding to these points are given in Tables 4 and 5 for buoyancy assisting and opposing flow respectively for different parameters. Similar profiles are obtained for $Pr = 3$ and 7 in Fig. 10(a), (b) for buoyancy assisting and opposing flow, respectively. The critical predominate values are tabulated in Tables 4 and 5.

5. Conclusions

The results show that as $|\theta_r|$ decreases (for fixed λ) the hydrodynamic boundary layer thickness decreases however,

Table 5
Critical values of $\lambda_{(\mathrm{crt.})s}$ for predominate buoyancy opposing shear stress at the surface and the corresponding $C_f Re^{0.5}$ for $Pr = 0.72$, 3, and 7.0 for various values of θ_r

θ_r	$Pr = 0.72$		$Pr = 3.0$		$Pr = 7.0$	
	$\lambda_{(\mathrm{crt.})s}$	$C_f Re^{0.5}$	$\lambda_{(\mathrm{crt.})s}$	$C_f Re^{0.5}$	$\lambda_{(\mathrm{crt.})s}$	$C_f Re^{0.5}$
10.0	−0.019	−0.97022	−0.0391	−0.95844	−0.0582	−0.95192
7.0	−0.0191	−0.98723	−0.0395	−0.97039	−0.0585	−0.96074
4.0	−0.0199	−1.03424	−0.040	−1.00109	−0.0593	−0.98349
2.0	−0.022	−1.16805	−0.0425	−1.08337	−0.062	−1.04169
1.1	−0.027	−1.50561	−0.044	−1.25262	−0.67	−1.15446
−0.1	–	–	−0.0125	−0.30244	−0.024	−0.33211
−0.5	–	–	−0.027	−0.61285	−0.044	−0.66205
−1.0	–	–	−0.032	−0.73517	−0.05	−0.77249
−4.0	−0.0168	−0.85176	−0.0354	−0.87212	−0.055	−0.88559
−7.0	−0.017	−0.88313	−0.0372	−0.89669	−0.056	−0.90485
−10.0	−0.0175	−0.89758	−0.0375	−0.90692	−0.056	−0.91252

the thermal boundary layers (TBL) thickness increase before λ reaches a specific value and after that the TBL decrease. The $Nu_x Re_x^{-1/2}$ is highly affected by the variable viscosity model for small values of $|\theta_r|$. However, for large $|\theta_r|$ the magnitude of $Nu_x Re_x^{-1/2}$ is independent of it and approaches its value at constant viscosity model corresponding to Pr and λ. On the other hand, increasing λ (for fixed $|\theta_r|$) enhances the heat transfer coefficient for all Prandtl numbers. However, at a specific value of λ, where the competition between the effect of variable viscosity and buoyancy is balanced, the $Nu_x Re_x^{-1/2}$ is almost independent of $|\theta_r|$. Otherwise, these profiles depend on θ_r in the forced convection region and on θ_r and λ in the natural convection region. Critical values of buoyancy assisting and opposing flow are obtained for predominate natural convection flow using θ_r as a parameter. Introducing the variable viscosity effect for large λ reduces the shear stress at the surface for $\theta_r < 0$ as θ_r tends to zero. However, at small λ the effect of variable viscosity is to increase the shear stress for assisting flow. Finally critical values of λ, corresponding to predominate buoyancy assisting and opposing effect on the dimensionless shear stress, are tabulated for different Prandtl number and viscosity/temperature parameter θ_r.

Acknowledgement

This research is supported by the College of Engineering Research Center at King Saud University under the project number 20/424. This support is highly appreciated and acknowledged.

References

[1] T. Altan, S. Oh, H. Gegel, Metal Forming Fundamentals and Applications, American Society of Metals, Metals Park, OH, 1979.
[2] E.G. Fisher, Extrusion of Plastics, Wiley, New York, 1976.
[3] Z. Tadmor, I. Klein, Engineering Principles of Plasticating Extrusion, Polymer Science and Engineering Series, Van Nostrand Reinhold, New York, 1970.
[4] B.C. Sakiadis, Boundary layer behavior on continuous solid surfaces: I. Boundary-layer equations for two-dimensional and axisymmetric flow, AIChE J. 7 (1) (1961) 26–28.
[5] F.K. Tsou, E.M. Sparrow, R.J. Goldstein, Flow and heat transfer in the boundary layer on a continuous moving surface, Internat. J. Heat Mass Transfer 10 (1967) 219–235.
[6] L.J. Crane, Flow past a stretching plane, Z. Angew. Math. Phys. 21 (1970) 645–647.
[7] L.G. Grubka, K.M. Bobba, Heat transfer characteristics of a continuous stretching surface with variable temperature, ASME J. Heat Transfer 107 (1985) 248–250.
[8] V.M. Soundalgekar, T.V. Ramana Murty, Heat transfer past a continuous moving plate with variable temperature, Wärme- und Stoffübertragung 14 (1980) 91–93.
[9] J. Vleggaar, Laminar boundary layer behavior on continuous accelerating surfaces, Chem. Engrg. Sci. 32 (1977) 1517–1525.
[10] M.E. Ali, Heat transfer characteristics of a continuous stretching surface, Wärme- und Stoffübertragung 29 (1994) 227–234.
[11] W.H.H. Banks, Similarity solutions of the boundary-layer equations for a stretching wall, J. Mec. Theor. Appl. 2 (1983) 375–392.
[12] M.E. Ali, The effect of suction or injection on the laminar boundary layer development over a stretched surface, J. King Saud University Eng. Sci. 8 (1) (1996) 43–58.
[13] E. Magyari, B. Keller, Heat and mass transfer in the boundary layers on an exponentially stretching continuous surface, J. Phys. D: Appl. Phys. 32 (1999) 577–585.
[14] E. Magyari, B. Keller, Heat transfer characteristics of the separation boundary flow induced by a continuous stretching surface, J. Phys. D: Appl. Phys. 32 (1999) 2876–2881.
[15] L.E. Erickson, L.T. Fan, V.G. Fox, Heat and mass transfer on a moving continuous flat plate with suction or injection, Indust. Engrg. Chem. Fundamentals 5 (1966) 19–25.
[16] V.G. Fox, L.E. Erickson, L.T. Fan, Methods for solving the boundary layer equations for moving continuous flat surfaces with suction and injection, AIChE J. 14 (1968) 726–736.
[17] P.S. Gupta, A.S. Gupta, Heat and mass transfer on a stretching sheet with suction or blowing, Canad. J. Chem. Engrg. 55 (6) (1977) 744–746.
[18] C.K. Chen, M.I. Char, Heat transfer of a continuous stretching surface with suction or blowing, J. Math. Anal. Appl. 135 (1988) 568–580.
[19] M.E. Ali, On thermal boundary layer on a power-law stretched surface with suction or injection, Internat. J. Heat Fluid Flow 16 (4) (1995) 280–290.
[20] E. Magyari, M.E. Ali, B. Keller, Heat and mass transfer characteristics of the self-similar boundary-layer flows induced by continuous surface stretched with rapidly decreasing velocities, Heat Mass Transfer 38 (2001) 65–74.
[21] H.T. Lin, K.Y. Wu, H.L. Hoh, Mixed convection from an isothermal horizontal plate moving in parallel or reversely to a free stream, Internat. J. Heat Mass Transfer 36 (1993) 3547–3554.
[22] M.E. Ali, F. Al-Yousef, Heat transfer and flow field on an extruded vertical material, in: Proceedings of the 10th Int. Conference of Mech. Power Engineering, Assiut University, Assiut, Egypt, 16–18 December, 1997, pp. 207–219.
[23] M.E. Ali, F. Al-Yousef, Laminar mixed convection from a continuously moving vertical surface with suction or injection, Heat Mass Transfer 33 (4) (1998) 301–306.
[24] M.E. Ali, F. Al-Yousef, Laminar mixed convection boundary layers induced by a linearly stretching permeable surface, Internat. J. Heat Mass Transfer 45 (2002) 4241–4250.
[25] C.H. Chen, Laminar mixed convection adjacent to vertical continuously stretching sheet, Heat Mass Transfer 33 (1998) 471–476.
[26] C.H. Chen, Mixed convection cooling of a heated continuously stretching surface, Heat Mass Transfer 36 (2000) 79–86.
[27] M.E. Ali, The buoyancy effects on the boundary layers induced by continuous surfaces stretched with rapidly decreasing velocities, Heat Mass Transfer 40 (2004) 285–291.

[28] H. Herwig, G. Wickern, The effect of variable properties on laminar boundary layer flow, Wärme- und Stoffübertragung 20 (1986) 47–57.
[29] I. Pop, R.S.R. Gorla, M. Rashidi, The effect of variable viscosity on flow and heat transfer to a continuous moving flat plate, Internat. J. Engrg. Sci. 30 (1) (1992) 1–6.
[30] E.M.A. Elbashbeshy, M.A.A. Bazid, The effect of temperature-dependent viscosity on heat transfer over a continuous moving surface, J. Phys. D: Appl. Phys. 33 (2000) 2716–2721.
[31] J.X. Ling, A. Dybbs, Forced convection over a flat plate submersed in a porous medium: Variable viscosity case, ASME Paper 87-WA/HT-23, ASME winter annual meeting, Boston, Massachusetts, December 1987, pp. 13–18.
[32] F.C. Lai, F.A. Kulacki, The effect of variable viscosity on convective heat transfer along a vertical surface in a saturated porous medium, Internat. J. Heat Mass Transfer 33 (5) (1990) 1028–1031.
[33] Md.A. Hossain, Md.S. Munir, I. Pop, Natural convection flow of a viscous fluid with viscosity inversely proportional to linear function of temperature from a vertical wavy cone, Internat. J. Thermal. Sci. 40 (2001) 366–371.
[34] Md.A. Hossain, Md.S. Munir, Mixed convection flow from a vertical flat plate with temperature dependent viscosity, Internat. J. Thermal. Sci. 39 (2000) 173–183.
[35] W.M. Kays, M.E. Crawford, Convective Heat and Mass Transfer, second ed., McGraw-Hill, New York, 1987.
[36] L.C. Burmeister, Convective Heat Transfer, Wiley, New York, 1983.